Exact two-electron wave packet dynamics of H2 in an intense laser field: Formation of localized ionic states H+ H-

doi: 10.1063/1.1319348

Exact two-electron wave packet dynamics of H_2 in an intense laser field: Formation of localized ionic states H^+H^-

Kenji Harumiya, Isao Kawata, Hirohiko Kono,[a] and Yuichi Fujimura
Department of Chemistry, Graduate School of Science, Tohoku University, Graduate School of Science, Sendai 980-8578, Japan

(Received 13 July 2000; accepted 29 August 2000)

We have developed an efficient grid method that can accurately deal with the electronic wave packet dynamics of two-electron systems in three-dimensional (3D) space. By using the dual transformation technique, we remove the numerical difficulties arising from the singularity of the attractive Coulomb potential. Electron–electron repulsion is incorporated into the wave packet propagation scheme without introducing any approximations. The exact electronic dynamics of H_2 is simulated for the first time. At small internuclear distances (e.g., $R=4$ a.u.), an ionic component characterized by the structure H^+H^- is created in an intense laser field $\mathcal{E}(t)$ (intensity $>10^{13}$ W/cm^2 and $\lambda \approx 720$ nm) because an electron is transferred from the nucleus around which the dipole interaction energy for the electron becomes higher with increasing $|\mathcal{E}(t)|$. The localized ionic structure is identified with the H^- anion at the nucleus around which the dipole interaction energy becomes lower. Tunneling ionization proceeds via the formation of such a localized ionic structure, and direct ionization from the covalent structure is much smaller; the localized ionic structure plays the dominant doorway state to ionization of H_2. © *2000 American Institute of Physics.* [S0021-9606(00)00544-4]

I. INTRODUCTION

The development of high-power lasers has opened up a research field of new nonperturbative phenomena in intense fields such as above-threshold ionization and higher-order harmonic generation of emission.[1–3] In the high-intensity and low-frequency regime (intensity $I>10^{13}$ W/cm^2 and wavelength $\lambda \approx 800$ nm), the Coulomb potential distorted by the laser electric field forms a ''quasistatic'' barrier (or barriers) through which an electron can tunnel.[4] For the case of atoms, such nonperturbative phenomena can be understood in terms of quasistatic plasma physics models.[5] A novel nonperturbative phenomenon peculiar to molecules, known as enhanced ionization, has also been discovered. Recent accurate numerical simulations of ionization for one-electron systems such as H_2^+ and H_3^{+2} have shown that the ionization rate has the maximum at a critical internuclear distance R_c and far exceeds that of the neutral fragment H.[6–8] Maxima in the ionization rate with respect to the internuclear distance R have also been found for two-electron model systems such as H_2 and H_4^{+2} in one-dimensional (1D) space.[9] In the calculations, the two electrons are allowed to move only along the molecular axis. Although the calculation of the ionization rate is limited to these one- or two-electron systems, enhanced ionization has been experimentally observed for various molecules[10] such as CO_2.[11]

As described in the next two paragraphs, it has been revealed that the enhanced ionization in H_2^+ is due to the suppression of electron transfer between the nuclei (called charge resonance enhanced ionization[6,8]). For the case of two-electron molecules, however, different mechanisms can be expected because the two electrons are forced to move in a correlative way by the laser field. In a previous paper,[12] we analyzed the ionization process for a 1D H_2 in an intense, low-frequency laser field (intensity $I \geqslant 10^{14}$ W/cm^2 and $\lambda = 1064$ nm) by numerically solving the time-dependent Schrödinger equation. According to the 1D model calculation, the laser field forces the two electrons to stay near a nucleus for a half cycle, and resultant transient ionic structures such as H^-H^+ and H^+H^- are the main doorway states to tunneling ionization. In this paper, we present the results of calculation of electronic wave packet dynamics of H_2 in a *three-dimensional* space to show that the formation of localized ionic states is real and that ionization mainly occurs therefrom.

The system H_2^+ is regarded as a prototype of odd-electron diatomic molecules. The electronic dynamics of H_2^+ prior to tunneling ionization is determined by the radiative coupling between the highest occupied molecular orbital (HOMO) and the lowest unoccupied molecular orbital (LUMO), $1\sigma_g$ and $1\sigma_u$, respectively.[6,7,13] The transition moment between them, parallel to the molecular axis, increases as $R/2$. This large transition moment is characteristic of a charge resonance transition between a bonding and a corresponding antibonding molecular orbital, which was originally pointed out by Mulliken.[14] The strong radiative coupling of the charge resonance transition changes the potential surfaces of $1\sigma_g$ and $1\sigma_u$ to ''field-following'' time-dependent adiabatic surfaces, i.e., $E_{\mp}(R) \approx I_p(\mathrm{H}) \mp \mathcal{E}(t)R/2$,[13] where $\mathcal{E}(t)$ is the laser electric field at time t and $I_p(\mathrm{H})$ is the ionization potential of H.

The instantaneous electrostatic potential for the electron in H_2^+ has two wells around the nuclei. The dipole interaction

[a]Electronic mail: kono@mcl.chem.tohoku.ac.jp

energy for an electron is $\mathcal{E}(t)R/2$ at the right nucleus and $-\mathcal{E}(t)R/2$ at the left nucleus. As $\mathcal{E}(t)$ increases from zero, the potential well formed around the right nucleus ascends and the well formed around the left nucleus descends.[13] Therefore, the ascending and descending wells yield the adiabatic energies E_+ and E_-, respectively. There exist barriers between the two wells and outside the descending well. While E_- is usually below the barrier heights, E_+ can be higher than the barrier heights in the range $R_c=7$ to 8 a.u.[15] In this critical range of R, the upper adiabatic state $|+\rangle$ is easier to ionize than is $|-\rangle$. These R_c values are consistent with the numerical simulations of ionization.[6,7] After one-electron ionization from H_2, the bond distance of the resultant H_2^+ stretches on the E_- laser-induced dissociative potential (bond softening due to the laser field)[16–18] and then the ionization proceeds via the $|+\rangle$ state which is nonadiabatically created around R_c from $|-\rangle$ when the field $\mathcal{E}(t)$ changes its sign. This mechanism of enhanced ionization has been directly proved by monitoring the populations of field-following adiabatic states such as $|+\rangle$ and $|-\rangle$.[13,15] A nonadiabatic transition between $|+\rangle$ and $|-\rangle$ corresponds to the spatial localization of the electron near a nucleus. The extra degree of freedom arising from nuclear motion necessitates the use of new concepts such as avoided potential crossings in a laser field. Field-induced nonadiabatic transitions through crossing points, as well as nuclear-motion induced ones, are essential for describing the electronic and nuclear dynamics in intense fields.[13,19,20]

We expect that the mechanism of enhanced ionization in two-electron diatomic molecules differs from that in the one-electron case: The excited ionic state H^-H^+ expected as the dominant doorway state to ionization can cross the covalent ground state H·H in field-following adiabatic energy. According to the results of 1D H_2 calculation,[12] as R decreases, the population of the localized ionic structure created increases. On the other hand, with decreases in R, the ionization rate from a pure H^-H^+ structure decreases owing to the stronger attraction by the distant nucleus. As a result, the rate has a peak at the critical distance $R_c \approx 6$ a.u.

In the 1D model, the Coulomb potentials are regularized; the two parameters ρ_{en} and ρ_{ee} are introduced to soften the electron–nucleus Coulomb potentials and the electron–electron repulsion potential, respectively.[9] The 1D calculated surfaces qualitatively agree with the experimental results, except that the 1D potentials are all shifted down. The transition moment between the 1D exact ground $1\sigma_g^2(X\,^1\Sigma_g^+)$ and first excited $1\sigma_g 1\sigma_u$ $(B\,^1\Sigma_u^+)$ states increases as $R/\sqrt{2}$ up to $R\approx 3$ a.u. (known as an electron transfer transition[14]) and converges to $\sqrt{2}\times$(atomic value). This is consistent with accurate calculations for 3D H_2.[21] Such large transition moments play the decisive role in the intense field case. Although these features validate the 1D model, 3D calculation is indispensable for quantitative discussions. Generally speaking, exact 3D calculation and 1D regularized model give different populations of H^-H^+ and different ionization rates from the pure H^-H^+. The localized ionic H^-H^+ structure geometrically has more different forms in 3D than in 1D. To understand the ionization processes of two-electron systems in detail, the 3D spatial configuration of the two electrons prior to ionization should be determined.

Electronic wave packet calculation for two-electron systems in 3D has, however, not yet been established, despite its pressing need.[22] To our knowledge, no wave packet calculations have been reported for two-electron molecules. Conventional time evolution methods using grid representations,[23] such as split operator techniques combined with fast Fourier transform,[24,25] have been successfully applied to the propagation of nuclear wave packets on adiabatic or diabatic potential surfaces. The success is attributed to the nonsingularity that internuclear potentials are usually expressed in terms of analytic functions of internuclear distances. On the other hand, for electronic dynamics, one must cope with the awkward Coulomb potential characterized by its long range and its singularity at the origin (e.g., at the nucleus for electron–nucleus interaction). The grid boundary in coordinate space must be chosen to be far from the origin to accommodate the wave function. For an attractive Coulomb potential, grid spacings must be small to reproduce high momentum components generated near the origin. Because of these difficulties, the performance of the conventional grid methods is very poor for Coulomb systems.

Recently, we have been developing an efficient grid method, the ''dual transformation'' method,[26,27] to propagate the electronic wave packet of a system accurately. In this method, we transform both the wave function and Hamiltonian consistently to overcome the numerical difficulties arising from the nature of the Coulomb potentials. The transformed wave function is required to be analytic so that the finite difference method works well. We have applied the method to one-electron systems such as H and H_2^+.[13,26,27] In this paper, we introduce the idea of dual transformation to deal with two-electron dynamics. The electron–electron interaction is fully taken into account.

The rest of this paper is organized as follows. Derivation of an H_2 Hamiltonian suitable for calculating the wave packet dynamics in an intense laser field is presented in Sec. II. In Sec. III, the dual transformation technique is applied to the time-dependent Schrödinger equation for the H_2 Hamiltonian derived in Sec. II. We describe the procedure for solving the transformed Schrödinger equation which the transformed wave function obeys. In Sec. IV, we demonstrate that in H_2 a localized ionic structure is created in an intense field and acts as the dominant doorway state to ionization. The 3D spatial configuration of the localized ionic structure is analyzed. Finally, in Sec. V, concluding remarks together with a brief summary of the present work is given.

II. DERIVATION OF A HAMILTONIAN OF H_2

We will describe the derivation of an H_2 Hamiltonian suitable for calculating the electronic wave packet dynamics in an intense laser field. The position of each electron is designated by cylindrical coordinates (ρ, z, and φ), as shown in Fig. 1. The z axis is parallel to the molecular axis. Here, we assume that the two nuclei are fixed in space at a given internuclear distance R and that the molecule is aligned by a linearly polarized laser electric field $\mathcal{E}(t)$ (the z axis is thus

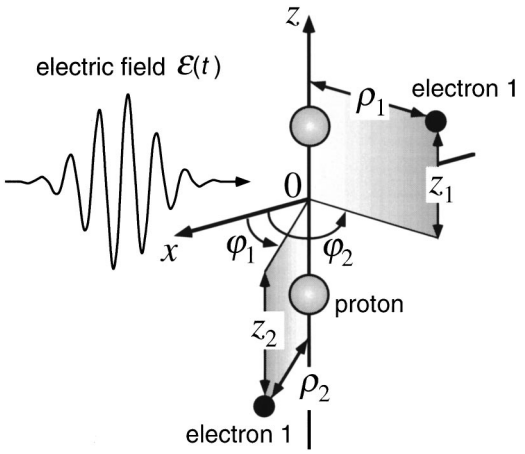

FIG. 1. Cylindrical coordinates (ρ_1, z_1, and φ_1) and (ρ_2, z_2, and φ_2) of the two electrons, 1 and 2, in H_2. The molecular axis is assumed to be parallel to the polarization direction of the laser electric field schematically illustrated with a sinusoidal line.

parallel to the polarization direction).[28,29] We first define a one-electron Hamiltonian $\hat{H}_j$ for the jth electron

$$\hat{H}_j = -\frac{1}{2}\left(\frac{\partial^2}{\partial\rho_j^2} + \frac{1}{\rho_j}\frac{\partial}{\partial\rho_j} + \frac{\partial^2}{\partial z_j^2}\right) + V(\rho_j, z_j) + z_j\mathcal{E}(t), \tag{1}$$

where the last term is the dipole interaction of the jth electron with the field $\mathcal{E}(t)$, and $V(\rho_j, z_j)$ represents the Coulomb attraction between the jth electron and the nuclei:

$$V(\rho, z) = -\frac{1}{\sqrt{\rho^2 + (z - R/2)^2}} - \frac{1}{\sqrt{\rho^2 + (z + R/2)^2}}. \tag{2}$$

Throughout this paper, atomic units are used unless otherwise noted.

If the kinetic energy associated with the z component of the angular momentum, $-(\frac{1}{2}\rho_j^2)\partial^2/\partial\varphi_j^2$, is added to $\hat{H}_j$, we obtain the Hamiltonian of H_2^+.[13] Thus, the total Hamiltonian of H_2 can be expressed as

$$\hat{H} = \sum_{j=1}^{2}\hat{H}_j + \left[-\left(\sum_{j=1}^{2}\frac{1}{2\rho_j^2}\frac{\partial^2}{\partial\varphi_j^2}\right) + V_{12}(\{\rho_j\},\{z_j\},\{\varphi_j\})\right], \tag{3}$$

where V_{12} is the electron–electron repulsion

$$V_{12}(\{\rho_j\},\{z_j\},\{\varphi_j\}) = \frac{1}{\sqrt{\rho_1^2 + \rho_2^2 - 2\rho_1\rho_2\cos(\varphi_1 - \varphi_2) + (z_1 - z_2)^2}}. \tag{4}$$

The Hamiltonian for He is obtained by setting R to zero. Introducing the relative angle ϕ between the two electrons,

$$\phi = \varphi_1 - \varphi_2, \tag{5}$$

and the average χ,

$$\chi = (\varphi_1 + \varphi_2)/2, \tag{6}$$

we can rewrite the two-electron part $[\cdots]$ in Eq. (3) as

$$\hat{H}_{12} = -\frac{1}{2}\left(\frac{1}{\rho_1^2} + \frac{1}{\rho_2^2}\right)\left(\frac{\partial^2}{\partial\phi^2} + \frac{\partial^2}{4\partial\chi^2}\right) - \frac{1}{2}\left(\frac{1}{\rho_1^2} - \frac{1}{\rho_2^2}\right)\frac{\partial}{\partial\chi}\frac{\partial}{\partial\phi} + V_{12}(\{\rho_j\},\{z_j\},\phi). \tag{7}$$

Since the molecular axis component of the total angular momentum is conserved, the wave function takes the product form of $e^{il\chi}$ and a function $\Phi(\{\rho_j\},\{z_j\},\phi)$, where l is the quantum number for the z component of the total angular momentum. The range of χ is between 0 and 2π: The allowed values are $l = 0, \pm 1, \pm 2, \ldots$. We denote the total Hamiltonian for $\Phi(\{\rho_j\},\{z_j\},\phi)$ by $\hat{H}(l)$

$$\hat{H}(l) = \hat{H}_{12}(l) + \sum_{j=1}^{2}\hat{H}_j, \tag{8}$$

where the two-electron part $\hat{H}_{12}(l)$ is

$$\hat{H}_{12}(l) = -\frac{1}{2}\left(\frac{1}{\rho_1^2} + \frac{1}{\rho_2^2}\right)\left(\frac{\partial^2}{\partial\phi^2} - \frac{l^2}{4}\right) - \frac{il}{2}\left(\frac{1}{\rho_1^2} - \frac{1}{\rho_2^2}\right)\frac{\partial}{\partial\phi} + V_{12}(\{\rho_j\},\{z_j\},\phi). \tag{9}$$

The Hamiltonian $\hat{H}(l)$ does not contain differentials with χ but has the quantum number l. When the state is a singlet, the wave function has the exchange symmetry $\Phi(\rho_1,\rho_2,z_1,z_2,\phi) = \Phi(\rho_2,\rho_1,z_2,z_1,-\phi)$ $[= \Phi(\rho_1,\rho_2,z_1,z_2,-\phi)$ for $l = 0]$.

III. DUAL TRANSFORMATION FOR WAVE PACKET PROPAGATION

Recently, we have been developing an efficient grid method for accurate propagation of an electronic wave packet.[26,27] In this method, called dual transformation, the following three requirements are introduced to treat an attractive Coulomb potential which is characterized by its long range and its singularity at the nucleus. The first one is as follows: (i) The wave function is transformed so that it is zero at the Coulomb singular points (which ensures that the numerical difficulties concerning singularity are avoided). The choice of new scaled coordinates is also crucial: (ii) Near the nuclei, the equally spaced intervals in the new (scaled) coordinates must generate small grid spacings in the linear scaled (cylindrical) coordinates (to cope with the extremely high momentum components near the nuclei); in the weak potential region where the distance from the nuclei is larger, the corresponding intervals in the linear scaled (cylindrical) coordinates are chosen to be relatively large and nearly constant. The transformed Schrödinger equation which the transformed wave function obeys is discretized in space with the help of finite difference formulas, and it is integrated in time by the alternating-direction implicit method (ADI).[30–32] To that end, the transformed wave function must be analytic around the nuclei: (iii) The differential operators contained in the transformed Hamiltonian can be evaluated well by the finite difference method even near the Coulomb singular points.

We have applied the method to H and H_2^+ (including molecular vibration),[26,27] where the unscaled cylindrical coordinate ρ is transformed to $\rho=f(\xi)$ so that the function f is chosen to satisfy the three requirements (i)–(iii) given above. In the case of a cylindrical coordinate system, the finite difference method does not provide sufficient accuracy for evaluating the differential operators contained in the Hamiltonian. Scaling can be extended to the unscaled z coordinate as $z=g(\zeta)$. The introduction of these transformations drastically reduces the required numbers of grid points. The propagation scheme obtained is numerically stable.

We apply the dual transformation technique to the following Schrödinger equation:

$$i\frac{\partial}{\partial t}\Phi(\{\rho_j\},\{z_j\},\phi)=\hat{H}(l)\Phi(\{\rho_j\},\{z_j\},\phi). \tag{10}$$

As in previous papers,[13,27] we transform the Hamiltonian $\hat{H}(l)$ by introducing the generalized cylindrical coordinate system as

$$\rho_j=f(\xi_j);\quad z_j=g(\zeta_j), \tag{11}$$

where f and g are functions of scaled coordinates ξ_j and ζ_j [$f(\xi_j)=\xi_j$ and $g(\zeta_j)=\zeta_j$ lead to ordinary cylindrical coordinates].

In addition to the variable transformation in $\hat{H}(l)$, we have to transform the wave function to avoid the numerical difficulties concerning Coulomb singularities. The original wave function $\Phi(\{\rho_j\},\{z_j\},\phi)$ which is in general finite at the nuclei must be transformed to a function $\Psi(\{\xi_j\},\{\zeta_j\},\phi)$ that is zero at the nuclei. This demand on the transformed wave function, i.e., requirement (i), must be satisfied under a normalization condition. The original wave function $\Phi(\{\rho_j\},\{z_j\},\phi)$ is normalized as

$$\int_0^\infty d\rho_1\int_0^\infty d\rho_2\int_{-\infty}^\infty dz_1\int_{-\infty}^\infty dz_2\int_0^{2\pi}d\phi\rho_1\rho_2 \times|\Phi(\{\rho_j\},\{z_j\},\phi)|^2=1. \tag{12}$$

When the finite difference method is used, it is generally difficult to conserve the norm of the wave function. For instance, the finite difference representation of $(1/\rho)\partial/\partial\rho$ in Eq. (1) is asymmetric, i.e., it is no longer Hermitian. It has been shown[26] that to make a time evolution scheme based on the finite difference method stable and accurate, the following normalization condition should be imposed on the transformed wave function $\Psi(\{\xi_j\},\{\zeta_j\},\phi)$ used in the actual numerical calculation

$$\int_0^\infty d\xi_1\int_0^\infty d\xi_2\int_{-\infty}^\infty d\zeta_1\int_{-\infty}^\infty d\zeta_2\int_0^{2\pi}d\phi \times|\Psi(\{\xi_j\},\{\zeta_j\},\phi)|^2=1. \tag{13}$$

Note that the scale factor for each coordinate or the Jacobian is formally unity.

The transformed wave function that satisfies the normalization condition, Eq. (13), is uniquely determined as

$$\Psi(\{\xi_j\},\{\zeta_j\},\phi)=[\Pi_{j=1}^2 f(\xi_j)f'(\xi_j)g'(\zeta_j)]^{1/2} \times\Phi(\{f(\xi_j)\},\{g(\zeta_j)\},\phi), \tag{14}$$

where a prime denotes the derivative with respect to the argument of the function. Inserting Eq. (14) into Eq. (10), we obtain the following transformed Schrödinger equation:

$$i\frac{\partial\Psi(\{\xi_j\},\{\zeta_j\},\phi)}{\partial t}=\hat{H}^T(l)\Psi(\{\xi_j\},\{\zeta_j\},\phi), \tag{15}$$

where the transformed Hamiltonian $\hat{H}^T(l)$ is expressed, in terms of the transformed ones, $\hat{H}_1^T$ and $\hat{H}_2^T$ for $\hat{H}_1$ and $\hat{H}_2$, as

$$\hat{H}^T(l)=\hat{H}_{12}(l)+\sum_{j=1}^2\hat{H}_j^T. \tag{16}$$

The explicit form of $\hat{H}_j^T$ is

$$\hat{H}_j^T=K_{\xi_j}+K_{\zeta_j}+V(f(\xi_j),g(\zeta_j))+g(\zeta_j)\mathcal{E}(t), \tag{17}$$

where K_ξ and K_ζ, i.e., the kinetic-energy parts with respect to coordinates ξ and ζ, are given by

$$K_\xi=-\frac{1}{2f'^2(\xi)}\left[\frac{\partial^2}{\partial\xi^2}-\frac{2f''(\xi)}{f'(\xi)}\frac{\partial}{\partial\xi}\right] +\frac{1}{4f'^4(\xi)}\left[\frac{5}{2}f''^2(\xi)-f'(\xi)f'''(\xi)\right]-\frac{1}{8f^2(\xi)}, \tag{18}$$

$$K_\zeta=-\frac{1}{4}\left[\frac{1}{g'^2(\zeta)}\frac{\partial^2}{\partial\zeta^2}+\frac{\partial^2}{\partial\zeta^2}\frac{1}{g'^2(\zeta)}\right] +\frac{1}{4g'^4(\zeta)}\left[\frac{7}{2}g''^2(\zeta)-g'(\zeta)g'''(\zeta)\right]. \tag{19}$$

It has been shown that the finite difference representations of K_ξ and K_ζ are nearly Hermitian.[27] The norm is practically conserved. The dual transformation is named after the two transformations, i.e., the variable transformation of the Hamiltonian and the transformation of the wave function with the normalization constraint Eq. (13).

The time evolution operator for $\Psi(\{\xi_j\},\{\zeta_j\},\phi)$ can be approximated as

$$\exp[-i\Delta t\hat{H}^T(l)]\approx[1+i\Delta t\hat{H}_{12}(l)/2]^{-1}U(\hat{H}_1^T)U(\hat{H}_2^T) \times[1-i\Delta t\hat{H}_{12}(l)/2], \tag{20}$$

where $U(\hat{H}_j^T)$ is an approximate time evolution operator for $\hat{H}_j^T$. As in previous papers,[26,27] we employ the Peaceman–Rachford formula,[33,34] which is a two-dimensional version of the ADI method

$$U(\hat{H}_j^T)=\frac{1}{(1+iA_j\Delta t/2)}\frac{(1-iB_j\Delta t/2)}{(1+iB_j\Delta t/2)}(1-iA_j\Delta t/2), \tag{21}$$

where

$$A_j=K_{\zeta_j}+V(f(\xi_j),g(\zeta_j))/2+g(\zeta_j)\mathcal{E}(t), \tag{22}$$

$$B_j=K_{\xi_j}+V(f(\xi_j),g(\zeta_j))/2. \tag{23}$$

The time evolution operators Eqs. (20) and (21) are accurate up to the order of Δt^2.

To fulfill the above three requirements, we employ the following form for $f(\xi)$, $f(\xi)=\xi\sqrt{\xi/(\xi+\alpha)}$, where parameter α is chosen so that $f(\xi)\approx\xi$ in the weak potential region.

In this paper, z_1 and z_2 are unscaled: $z_1=\zeta_1$ and $z_2=\zeta_2$. Around the singular points (located along $\xi=0$), the prefactor $\sqrt{ff'g'}$ in the transformed wave function Eq. (14) changes as $\approx\xi\sqrt{3/2\alpha}$, which meets requirements (i) and (iii). Inverting equally spaced points in ξ onto ρ, one finds that the grid spacing in ρ is proportional to f'. As ξ increases, f' changes from $(\frac{3}{2})\sqrt{\xi/\alpha}$ to 1. When α is much larger than the grid spacing $\Delta\xi$ and the attractive potential $V(f(\xi),g(\zeta))$ is nearly flat in the region where $\rho>f(\alpha)=\alpha/\sqrt{2}$, requirement (ii) is met. Then, the grid spacing along the ρ-direction decreases as the grid point approaches the singular points.

In addition to the dual transformation technique, we introduce a staggered point coordinate system for z_1 and z_2 to avoid the numerical divergence at the electron–electron coalescence. The coordinates z_1 and z_2 are unscaled but the grid points for the two coordinates are staggered; $z_1=n\Delta z$, $(n+1)\Delta z,\ldots$, and $z_2=(n+\frac{1}{2})\Delta z$, $(n+\frac{3}{2})\Delta z,\ldots$ (where n is an integer). In this way, the distance between the two electrons is kept from being zero. The grid representation of $\hat{H}_{12}(l)$ does not include an infinite value and causes no numerical difficulties.

All of the operators are converted to grid representations by the finite difference method. The operation of Eq. (20) on the wave function $\Psi(\{\xi_j\},\{\zeta_j\},\phi)$ is as follows. After the explicit application of $1-i\Delta t\hat{H}_{12}(l)/2$ in Eq. (20), we apply the Peaceman–Rachford implicit scheme to Eq. (21). The operation of $U(\hat{H}_j^T)$ on the wave function $\Psi(t_n)=[1-i\Delta t\hat{H}_{12}(l)/2]\Psi(\{\xi_j\},\{\zeta_j\},\phi)$ is separated into two steps by introducing an ''artificial'' intermediate state $\Psi^{n+1/2}$: $(1+iB_j\Delta t/2)\Psi^{n+1/2}=(1-iA_j\Delta t/2)\Psi(t_n)$ and $(1+iA_j\Delta t/2)\times[U(\hat{H}_j^T)\Psi(t)_n]=(1-iB_j\Delta t/2)\Psi^{n+1/2}$. The wave function $U(\hat{H}_j^T)\Psi(t_n)$ can be obtained by solving the two equations in order. Applying finite difference formulas to the two equations, we obtain two sets of systems of simultaneous linear algebraic equations for the unknown $\Psi^{n+1/2}$ and $U(\hat{H}_j^T)\Psi(t_n)$. The systems of equations are tridiagonal for the three-point finite difference representation and pentadiagonal for the five-point finite difference representation. The operation of $[1+i\Delta t\hat{H}_{12}(l)/2]^{-1}$ in the final stage can be calculated by the Cranck–Nicholson implicit scheme.[30,35]

IV. RESULTS AND DISCUSSION

We present an example of 3D wave packet dynamics at $R=4$ a.u., which is larger than the equilibrium internuclear distance. We assume that the initial state is the singlet ground state which has $l=0$. The ''exact'' ground state can be obtained by operating a Hanning spectral filter[24] $W(|\hat{H}^T(l=0)-E_0|)$ on an approximate ground-state Φ_A

$$W(|\hat{H}^T(l=0)-E_0|)=\int_0^\tau[1+\cos(\pi t/\tau)]\times\exp\{it[\hat{H}^T(l=0)-E_0]\}dt, \tag{24}$$

where $\mathcal{E}(t)$ in $\hat{H}^T(l=0)$ is set to zero. The filter W is a monotonically decreasing function and the width in energy is proportional to $1/\tau$. Using the trapezoidal rule for the above integration, the operation of W on Φ_A is reduced to operations of the propagator Eq. (20).[36] When E_0 is chosen to be near the exact ground-state energy, the operation of W on Φ_A diminishes the excited components in Φ_A. The energy of the wave function $W\Phi_A$ in the grid representation, E_0', is generally different from the initial guess E_0. The operation of W is repeated until E_0' is sufficiently close to E_0 (after each operation of W, E_0 is replaced with E_0'). The wave function obtained after convergence is the ground state of the discretized Hamiltonian. In this paper, we employ the following function as Φ_A:

$$\Phi_A(1,2)\propto a(1)b(2)+b(1)a(2), \tag{25}$$

where a and b denote the $1s$ atomic orbitals on the left proton a and the right proton b, respectively, and 1 and 2 represent the coordinates of the two electrons.

We use $\alpha=28.3$ a.u. for the variable transformation $f(\xi)$. Around this value (±10 a.u.), the results are insensitive to α.[27] In the region where $\rho>f(\alpha)=28.3/\sqrt{2}$ a.u., the Coulomb attractive potential is nearly flat. The grid spacings used are $\Delta\xi=0.328$ a.u. (which must be much smaller than α), $\Delta z=\Delta\zeta=0.4$ a.u., and $\Delta\phi=0.0982$. The grid end points are chosen as $\xi_{\max}=9.84$ a.u. (the corresponding grid end in ρ is $\rho_{\max}=5$ a.u.) and $z_{\max}\approx-z_{\min}\approx10$ a.u. At the grid boundaries, we set $\Psi(\{\xi_j\},\{\zeta_j\},\phi)=0$. The time step used is $\Delta t=0.02$–0.05 a.u. We use five-point finite difference representation. The energy of the ground state obtained by the operation of the energy filter Eq. (24) is $-1.015\,48$ a.u., while the exact one is $-1.016\,37$ a.u.[37] The obtained energy converges at the exact one as Δz and $\Delta\rho$ decrease under the condition that $\Delta z\geqslant\Delta\rho$. On this condition the change in the wave function along the ρ-coordinate is sufficiently smooth even near the electron–electron coalescence (i.e., the staggered coordinate system works well) and the numerical scheme is hence stable.

Electron transfer in H_2 can be characterized by the reduced density

$$\overline{P}(z_1,z_2)=\int_0^\infty d\rho_1\int_0^\infty d\rho_2\int_0^{2\pi}d\phi\rho_1\rho_2\times|\Phi(\rho_1,\rho_2,z_1,z_2,\phi)|^2. \tag{26}$$

The covalent component (H·H) around $z_1=-z_2=\pm R/2$ and the ionic components (H^-H^+ and H^+H^-) around $z_1=z_2=\pm R/2$ can be distinguished by using the representation Eq. (26). The field $\mathcal{E}(t)$ that the H_2 interacts with is assumed to be $f(t)\sin(\omega t)$, where ω is the frequency and the pulse envelope $f(t)$ is linearly ramped with time t so that after one cycle $f(t)$ attains its maximum $\mathcal{E}_0$. The field parameters used are as follows: $\mathcal{E}_0=0.12$ a.u. (intensity $I=5.04\times10^{14}$ W/cm^2) and $\omega=0.06$ a.u. ($\lambda=760$ nm). Snapshots of $\overline{P}(z_1,z_2)$ are drawn in Fig. 2: (a) $t=0$; (b) $t=\pi/2\omega=26.2$ a.u. (1 a.u.$=0.0242$ fs); (c) $t=\pi/\omega$; (d) $t=3\pi/2\omega$. For a singlet state, the exchange symmetry $\overline{P}(z_1,z_2)=\overline{P}(z_2,z_1)$ is maintained. The instantaneous field strength is $\mathcal{E}(t)=0.03$ a.u. ($I=3.15\times10^{13}$ W/cm^2) at $t=\pi/2\omega$; at $t=3\pi/2\omega$, $\mathcal{E}(t)=-0.09$ a.u. ($I=2.84\times10^{14}$ W/cm^2).

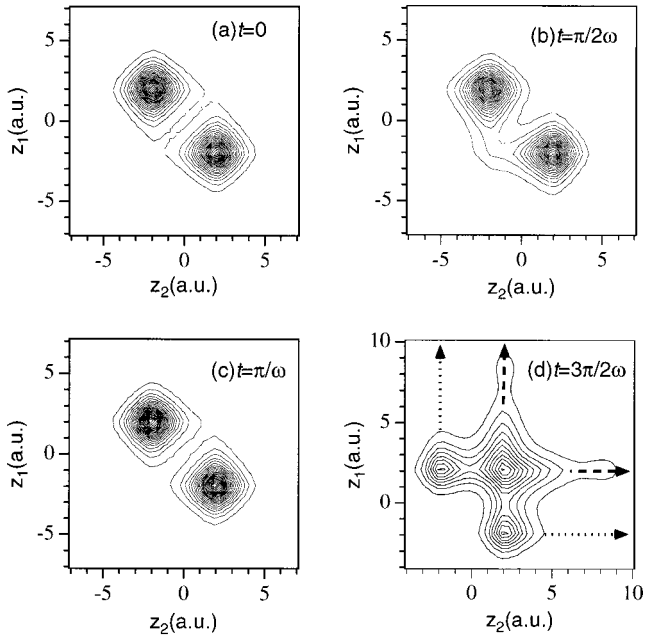

FIG. 2. Snapshots of the wave packet of the 3D H_2 in an intense field. The probability $\bar{P}(z_1,z_2)$ defined by Eq. (26) is drawn at quarter cycle intervals ($\omega=0.06$ a.u.): (a) $t=0$; (b) $t=\pi/2\omega=26.2$ a.u.; (c) $t=\pi/\omega$; (d) $t=3\pi/2\omega$. The contour intervals are the same for the four panels. The instantaneous field strength is $\mathcal{E}(t)=0.03$ a.u. at $t=\pi/2\omega$ and $\mathcal{E}(t)=-0.09$ a.u. at $t=3\pi/2\omega$. The wave packet can be characterized by the covalent component around $z_1=-z_2=\pm R/2$ and the ionic components around $z_1=z_2=\pm R/2$. An ionic component of the structure H^-H^+ or H^+H^- is created near the descending well [where $z\mathcal{E}(t)<0$, i.e., the descending well is formed around the left nucleus when $\mathcal{E}(t)>0$]. The ionic component at the left nucleus increases as the field approaches the first local maximum at $t=\pi/2\omega$, as shown in (b). A quarter cycle later, the field returns to zero. The packet at $t=\pi/\omega$ in (c) is nearly identical to the initial one in (a). In (d), the density around the ionic configuration $z_1=z_2=R/2$ becomes very high because of the stronger field strength at $t=3\pi/2\omega$. As indicated by the broken line in (d), an electron is ejected from the localized ionic structure. The direct ionization route from the covalent structure H·H is denoted by the dotted line in (d), but the ionization current along the dotted line is relatively small.

A comparison of Figs. 2(a) and 2(b) shows that the ionic component around the left nucleus, where $z_1=z_2=-R/2$, increases as the field approaches the first local maximum at $t=\pi/2\omega$. The ionic component created near the descending well [where $z\mathcal{E}(t)<0$] is a result of the laser-induced electron transfer from the ascending well. A quarter cycle later, the field returns to zero. The packet at $t=\pi/\omega$ in Fig. 2(c) is nearly identical with the initial one in Fig. 2(a), indicating that the response to the field is still adiabatic.[13,38] In Fig. 2(d), the density around $z_1=z_2=R/2$ becomes very high because of the stronger field strength at $t=3\pi/2\omega$. To quantify the localized ionic component created, we define the localized ionic structure $|H^+H^-\rangle$ and $|H^-H^+\rangle$ as the bound state H^- ions located at $z=\pm R/2$, respectively. At $t=0$, $|\langle\Phi|H^+H^-\rangle|^2=|\langle\Phi|H^-H^+\rangle|^2=0.19$. The ionic character increases as the field strength increases; at $t=3\pi/2\omega$, the ionic character is as large as $|\langle\Phi|H^+H^-\rangle|^2=0.54$. For the 1D regularized model with the conventionally used values of the softening parameters, i.e., for $\rho_{en}=\rho_{ee}=1$ a.u.,[9] $|\langle\Phi|H^+H^-\rangle|^2=|\langle\Phi|H^-H^+\rangle|^2=0.32$ at $t=0$ and $|\langle\Phi|H^+H^-\rangle|^2=0.64$ at $t=3\pi/2\omega$.

The field strength necessary for creating a localized ionic state, $\mathcal{E}_t$, is estimated as follows. The energy of the initial covalent state is roughly given by $-2I_p(H)$. The energy of the localized ionic state in the descending well at the field $\mathcal{E}(t)$, $E(H^+H^-)$, is

$$E(H^+H^-)\approx -I_p(H)-I_p(H^-)-1/R-|\mathcal{E}(t)|R, \tag{27}$$

where $I_p(H^-)=0.027$ a.u. is the ionization potential of H^-, $-1/R$ is the energy of the Coulomb attraction between H^- and H^+, and $-|\mathcal{E}(t)|R$ is the dipole interaction energy of the two charges in the descending well. A necessary condition for the formation of a localized ionic state is then given by $E(H^+H^-)\approx -2I_p(H)$. We thus have the critical intensity $\mathcal{E}_t$ as[12]

$$\mathcal{E}_t=[I_p(H)-I_p(H^-)-1/R]/R\approx[0.5-1/R]/R. \tag{28}$$

For $R=4$ a.u., $\mathcal{E}_t\approx 0.06$ a.u. The dramatic increase in the population of H^- shown in Fig. 2(d) can be explained by the fact that $|\mathcal{E}(t)|$ at $t=3\pi/2\omega$ is greater than $\mathcal{E}_t\approx 0.06$ a.u.

As indicated by the broken line in Fig. 2(d), an electron is ejected from the localized ionic structure. The ionic structure has a very low ionization potential as $I_p(H^-)$ and is hence regarded as a doorway state to ionization. The direct ionization route from the covalent structure H·H is denoted by the dotted line in Fig. 2(d), but the ionization current along the dotted line is relatively small. At $R=4$ a.u., the population of the localized ionic structure is more than 0.5 and the rate of ionization from the *pure* ionic state is greater than that from the *pure* covalent state. As R increases, the difference in the rate is expected to further increase because of the less attractive force of the distant nucleus. However, the population of the ionic component will decrease with increases in R.

We next examine the spatial configuration of the ionic structure at $t=3\pi/2\omega$. The spatial configuration of the two electrons at $z_1=z_2=R/2$ is given by

$$P(\rho_1,\rho_2,\phi)=\rho_1\rho_2|\Phi(\rho_1,\rho_2,z_1=R/2,z_2=R/2,\phi)|^2. \tag{29}$$

We show two typical cases of the configuration. One is the opposition configuration in which the two electrons are opposite to each other with respect to the right nucleus; i.e., $\phi=\pi$. The other is the case in which the two electrons are one sided; i.e., $\phi=0$. The two quantities $P(\rho_1,\rho_2,\phi=\pi)$ and $P(\rho_1,\rho_2,\phi=0)$ are plotted as functions of ρ_1 and ρ_2 in Figs. 3(a) and 3(b), respectively. The peak in Fig. 3(a) indicates a dominant configuration in which the two electrons in opposition to each other are ~0.8 a.u. away from the nucleus. As shown in Fig. 3(b), in the one-sided configuration, one electron is only 0.4 a.u. away from the nucleus and the other one is far away from the nucleus. The configuration of the unequal distances from the nucleus reduces the electron–electron repulsion energy. We also show the angle dependence of the two-electron configuration at $z_1=z_2=R/2$

$$\bar{P}(\phi)=\int_0^\infty d\rho_1\int_0^\infty d\rho_2\rho_1\rho_2|\Phi(\rho_1,\rho_2,z_1=R/2,z_2=R/2,\phi)|^2. \tag{30}$$

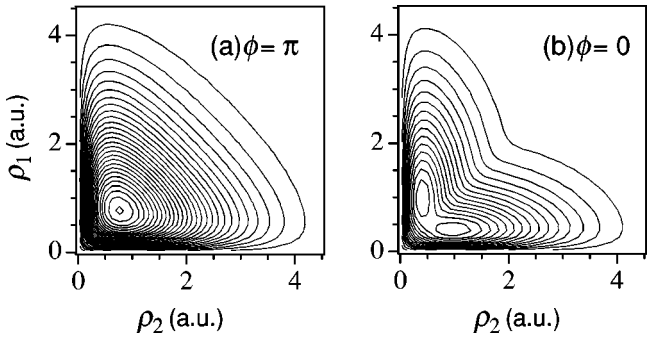

FIG. 3. Geometrical configuration of the localized ionic structure at $t=3\pi/2\omega$. The spatial configuration of the two electrons at $z_1=z_2=R/2$ defined by Eq. (29) is plotted as a function of ρ_1 and ρ_2 for two cases: (a) the two electrons being opposite to each other with respect to the right nucleus (i.e., $\phi=\pi$) and (b) the two electrons being one-sided (i.e., $\phi=0$). The peak in (a) indicates a dominant configuration in which the two electrons in opposition to each other are ~0.8 a.u. away from the nucleus. As shown in (b), in the one-sided configuration, one electron is only 0.4 a.u. away from the nucleus as and the other one is far away from the nucleus. The contour lines in (a) and (b) are plotted at the same intervals.

The results of analysis of the wave function at $t=3\pi/2\omega$ are plotted in Fig. 4. Because of the weaker electron–electron repulsion in the opposition configuration ($\phi=\pi$), $\bar{P}(\phi=\pi)$ is twice as large as the value in the one-sided configuration ($\phi=0$).

The geometrical structure of the created ionic state, which is shown in Figs. 3 and 4, is nearly identical to that of the pure H^- at the nucleus, which is consistent with the large overlap of Φ with H^-. The calculation for the bound state of H^- is performed with the same method described in this paper (by setting $R=0$ and unifying the two nuclei into one proton). In conclusion, in a small R (e.g., ~4 a.u.) region, the doorway state to ionization is the structure of the H^- ion at the nucleus where the dipole interaction energy for the electrons becomes lower with increasing $|\mathcal{E}(t)|$.

V. SUMMARY

We have developed an efficient grid method that can accurately deal with two-electron systems. Electron–electron repulsion is incorporated into the wave packet propagation scheme, in principle, without introducing any approximations. The positions of the two electrons, 1 and 2, are designated in terms of cylindrical coordinates (ρ_1,z_1,φ_1) and (ρ_2,z_2,φ_2). When the z component of the total angular momentum is conserved, the average $\chi=(\varphi_1+\varphi_2)/2$ can be practically eliminated from the Hamiltonian. This is the case for the H_2 molecule aligned in the polarization direction of the laser electric field. Then, the Hamiltonian contains five degrees of freedom $(\rho_1,\rho_2,z_1,z_2,\phi=\varphi_1-\varphi_2)$. By using the dual transformation technique, we have treated the awkward attractive Coulomb potentials and removed the numerical difficulties arising from their singular points.

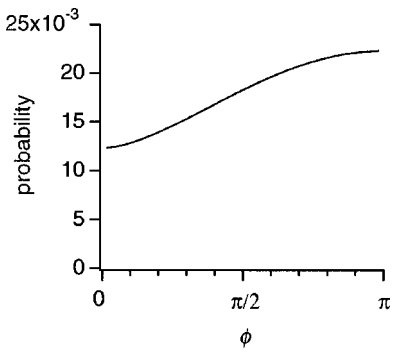

FIG. 4. Angle dependence of the two-electron configuration at $z_1=z_2=R/2$ for the wave function at $t=3\pi/2\omega$. The probability $\bar{P}(\phi)$ is defined by Eq. (30). The opposition configuration ($\phi=\pi$) takes a value that is twice as large as the one-sided configuration ($\phi=0$).

An example of the wave packet dynamics of H_2 at $R=4$ a.u. has been presented. An ionic component characterized by the structure H^+H^- is created near the descending well because of the laser-induced electron transfer from the ascending well (i.e., from the nucleus of the higher potential for the electron). Ionization proceeds via the formation of a localized ionic component in the *descending* well, in contrast to the H_2^+ case where the electron is ejected from the *ascending* well. For the case of $R=4$ a.u., one of the two electrons near a nucleus is transferred to the other nucleus when the field changes its sign. The return to the covalent state is accelerated by the electron–electron repulsion which is added to the attraction of the distant nucleus. As a result, nonadiabatic transitions of the electron pair from the descending well to the ascending well hardly occur. The direct ionization from the covalent state is much smaller than that from the ionic state created in the descending well. From 3D analysis of the spatial configuration of the two electrons, we identified the ionic structure with the H^- ion at the nucleus of the lower potential. On the basis of the results of 3D simulation, we conclude that the localized ionic structure characterized by H^- plays the role of dominant doorway state to ionization in the ''real'' H_2. In a future study, we will try to determine through what spatial configuration of the two electrons the ionization proceeds.

According to the 1D results in Ref. 12, the enhanced ionization is determined by the population of the main doorway state to ionization, H^-H^+, and the ionization probability from H^-H^+. As R increases, the population of the localized ionic structure created becomes smaller. At large internuclear distances ($R>10$ a.u.), ionization occurs from the covalent component (the ionization rate from the pure covalent structure is nearly independent of R), but the ionization rate is much smaller than a pure localized ionic structure. We are currently performing 3D calculations at different values of R to clarify the ionization mechanism in 3D two-electron systems and the possibility of two-electron simultaneous ionization. The work in progress will be reported elsewhere.

ACKNOWLEDGMENTS

This work was supported in part by the Development of High-Density Optical Pulse Generation and Advanced Material Control Techniques and by a grant-in-aid for scientific research from the Ministry of Education, Science and Cul-

ture, Japan (12640484). We would like to express our appreciation to Professor A. D. Bandrauk for his valuable discussion.

[1] M. Gavrila, *Atoms in Intense Fields* (Academic, New York, 1992).
[2] J. H. Eberly, J. Javanainen, and K. Rzazewski, Phys. Rep. **204**, 331 (1991); M. Lewenstein, K. C. Kulander, K. J. Schafer, and P. H. Bucksbaum, Phys. Rev. A **51**, 1495 (1995).
[3] K. Burnett, V. C. Reed, J. Cooper, and P. L. Knight, Phys. Rev. A **45**, 3347 (1992); J. L. Krause, K. J. Schafer, and K. C. Kulander, *ibid.* **45**, 4998 (1992); T. Zuo, A. D. Bandrauk, M. Ivanov, and P. B. Corkum, *ibid.* **51**, 3991 (1995); A. Rundquist, G. Durfee, III, Z. Chang, C. Herne, S. Backus, M. M. Murnane, and H. C. Kapteyn, Science **280**, 1412 (1998); M. Kakehata, H. Takada, K. Miyazaki, H. Kono, I. Kawata, and Y. Fujimura, Appl. Phys. B **70**, 219 (2000).
[4] L. V. Keldysh, Sov. Phys. JETP **20**, 1307 (1965); F. H. M. Faisal, J. Phys. B **6**, L89 (1973); H. R. Reiss, Phys. Rev. A **22**, 1786 (1980); S. Augst, D. D. Meyerhofer, D. Strickland, and S. L. Chin, J. Opt. Soc. Am. B **8**, 858 (1991); M. V. Ammosov, N. B. Delone, and V. P. Krainov, Sov. Phys. JETP **64**, 1191 (1986).
[5] P. B. Corkum, Phys. Rev. Lett. **71**, 1994 (1993).
[6] T. Zuo and A. D. Bandrauk, Phys. Rev. A **48**, 3837 (1993); S. Chelkowski and A. D. Bandrauk, J. Phys. B **28**, L723 (1995).
[7] T. Seidemann, M. Y. Ivanov, and P. B. Corkum, Phys. Rev. Lett. **75**, 2819 (1995).
[8] A. D. Bandrauk, Comments At. Mol. Phys. D **1**, 97 (1999); A. D. Bandrauk and J. Ruel, Phys. Rev. A **59**, 2153 (1999).
[9] H. Yu, T. Zuo, and A. D. Bandrauk, Phys. Rev. A **54**, 3290 (1996).
[10] J. H. Posthumus, A. J. Giles, M. R. Thompson, and K. Codling, J. Phys. B **29**, 5811 (1996); E. Constant, H. Stapelfelt, and P. B. Corkum, Phys. Rev. Lett. **76**, 4140 (1996); L. J. Frasinski, K. Codling, and P. Hatherly, *ibid.* **58**, 2424 (1989); K. Codling and L. J. Frasinski, J. Phys. B **26**, 783 (1993); C. Cornaggia, J. Lavancier, D. Normand, J. Morellec, and H. X. Liu, Phys. Rev. A **42**, 5464 (1990); M. Schmidt, D. Normand, and C. Cornaggia, *ibid.* **50**, 5037 (1994); G. N. Gibson, M. Li, C. Guo, and J. P. Nibarger, *ibid.* **58**, 4723 (1998).
[11] A. Hishikawa, A. Iwamae, and K. Yamanouchi, Phys. Rev. Lett. **83**, 1127 (1999); A. Iwamae, A. Hishikawa, and K. Yamanouchi, J. Phys. B **33**, 223 (2000).
[12] I. Kawata, H. Kono, Y. Fujimura, and A. D. Bandrauk, Phys. Rev. A **62**, 031401 (R) (2000).
[13] I. Kawata, H. Kono, and Y. Fujimura, J. Chem. Phys. **110**, 11152 (1999); I. Kawata, H. Kono, and Y. Fujimura, Chem. Phys. Lett. **289**, 546 (1998).
[14] R. S. Mulliken, J. Chem. Phys. **7**, 20 (1939).
[15] H. Kono and I. Kawata, in *Quantum Control of Chemical Recation Dynamics*, edited by R. J. Gordon and Y. Fujimura (World Scientific, Singapore), in press.
[16] A. Zavriyev, P. H. Bucksbaum, J. Squier, and F. Saline, Phys. Rev. Lett. **70**, 1077 (1993).
[17] B. Sheehy and L. F. DiMauro, Annu. Rev. Phys. Chem. **47**, 463 (1996).
[18] T. D. G. Walsh, F. A. Ilkov, S. L. Chin, F. Châteauneuf, T.-T. Nguyen-Dang, S. Chelkowski, A. D. Bandrauk, and O. Atabek, Phys. Rev. A **58**, 3922 (1998); T.-T. Nguyen-Dang, F. Châteauneuf, S. Manoli, O. Atabek, and A. Keller, *ibid.* **56**, 2142 (1997).
[19] A. D. Bandrauk, *Molecules in Intense Laser Fields* (Dekker, New York, 1994), Chaps. 1–3.
[20] P. Dietrich, M. Yu. Ivanov, F. A. Ilkov, and P. B. Corkum, Phys. Rev. Lett. **77**, 4150 (1996).
[21] L. Wolniewicz, J. Chem. Phys. **51**, 5002 (1969).
[22] For example, the mechanism of simultaneous two-electron ionization in atoms has not been solved yet. See W. C. Liu, J. H. Eberly, S. L. Haan, and R. Grobe, Phys. Rev. Lett. **83**, 520 (1999); Th. Weber, M. Weckenbrock, A. Staudte *et al.*, *ibid.* **84**, 443 (2000); R. Moshammer, B. Feuerstein, W. Schmitt *et al.*, Phys. Rev. Lett. **84**, 447 (2000).
[23] R. Kosloff, J. Phys. Chem. **92**, 2087 (1988); N. Balakrishnan, C. Kalyanaraman, and N. Sathyamurthy, Phys. Rep. **280**, 79 (1997).
[24] M. D. Feit, J. A. Fleck, Jr., and A. Steiger, J. Comput. Phys. **47**, 412 (1982); M. D. Feit and J. A. Fleck, Jr., J. Chem. Phys. **78**, 301 (1983).
[25] H. Kono and S. H. Lin, J. Chem. Phys. **84**, 1071 (1986).
[26] H. Kono, A. Kita, Y. Ohtsuki, and Y. Fujimura, J. Comput. Phys. **130**, 148 (1997).
[27] I. Kawata and H. Kono, J. Chem. Phys. **111**, 9498 (1999).
[28] B. Friedrich and D. Herschbach, Phys. Rev. Lett. **74**, 4623 (1995); H. Sakai, C. P. Safvan, J. J. Larsen, K. M. Hilligsøe, K. Hald, and H. Stapelfeldt, J. Chem. Phys. **110**, 10235 (1999); J. J. Larsen, H. Sakai, C. P. Safvan, Ida Wendt-Larsen, and H. Stapelfeldt, *ibid.* **111**, 7774 (1999).
[29] M. Schmidt, S. Dobosz, P. Meynadier, P. D'Oliveira, D. Normand, E. Charron, and A. Suzor-Weiner, Phys. Rev. A **60**, 4706 (1999).
[30] W. H. Press, S. A. Teukolsky, W. T. Vetterling, and B. P. Flannery, *Numerical Recipes in Fortran*, 2nd ed. (Cambridge, New York, 1992), Chap. 19.
[31] A. R. Mitchell, *Computational Methods in Partial Differential Equations* (Wiley, New York, 1969).
[32] N. N. Yanenko, *The Method of Fractional Steps* (Springer, New York, 1971).
[33] R. Varga, *Matrix Iterative Analysis* (Prentice-Hall, Englewood Cliffs, 1962), p. 273.
[34] D. M. Yang and R. T. Gregory, *A Survey of Numerical Mathematics, Vol. II* (Addison-Wesley, Reading, 1973), p. 1097.
[35] A. Askar and A. S. Cakmak, J. Chem. Phys. **68**, 2794 (1978).
[36] H. Kono and Y. Fujimura, Chem. Phys. Lett. **184**, 497 (1991).
[37] W. Kolos and Wolniewicz, J. Chem. Phys. **43**, 2429 (1965).
[38] Y. Kayanuma, Phys. Rev. B **47**, 9940 (1993); Phys. Rev. A **50**, 843 (1994).